Materials Advances

ROYAL SOCIETY OF CHEMISTRY

PAPER

View Article Online
View Journal | View Issue

Cite this: *Mater. Adv.*, 2025, 6, 1144

Role of metal atoms in the refractivity of cysteine- and phenylalanine-based metal–organic crystals†

Noam Brown, [ae] María Camarasa-Gómez, [d] Angelica Niazov-Elkan, [d] Ashwin Ramasubramaniam, [fg] Ehud Gazit, *[abc] Leeor Kronik *[d] and Oded Hod *[e]

Received 5th October 2024,
Accepted 27th December 2024

DOI: 10.1039/d4ma00999a

rsc.li/materials-advances

Refractive materials found in the natural world often exhibit unique structures that result in intriguing physical properties and offer a valuable resource for designing tailored bio-inspired materials. Here, we investigate from first principles the factors that govern the refractive index of metal–amino-acid crystals. We specifically focus on the influence of crystal structure, metal ion inclusion, and spin configuration in phenylalanine- and cysteine-based materials. We find that the inclusion of copper and zinc metal ions in the crystal lattice has an important structural role that directly influences the refractive properties. In addition, the metal ions may contribute significantly to the dielectric response and therefore to the refractive index even within a given structure. Furthermore, in the synthetically available case of phenylalanine–copper we verify the results experimentally. Our results demonstrate the role of the inclusion of metal atoms in biogenic assemblies, emphasizing the potential use of this concept in bio-inspired molecular crystals that offer a flexible platform for the design of novel materials with desired optical features.

1. Introduction

Bio-inspired materials generally attempt to exploit evolutionarily optimized structure-function relations found in nature, by incorporating natural components or motifs in order to achieve ease of fabrication and desired functionality. These materials often exhibit unique mechanical, electrical, optical, or magnetic properties, leading to novel applications.[1–6]

A particularly important function of biogenic materials, utilized by different classes of organisms, involves the use of optical refraction to facilitate vision, coloration, or camouflage.[7–10] These functionalities are usually enabled by molecular crystals, often packed in complex superstructures that reflect, refract, or scatter light.[11] Typically, such crystals incorporate organic molecules. The best-known example is guanine,[12–15] but other molecules, including isoxanthopterin, 7,8-dihydroxanthopterin, xanthine, riboflavin, and more, have also been identified.[9,16–19] This has spurred interest in high refractive index bio-inspired materials.[20–23]

Some optically relevant biogenic materials are known to incorporate metal moieties. For example, several melanin-based systems contain calcium, copper, or zinc ions.[24,25] Metallic moieties can also be involved in chemical reactions that produce pigments or in biomineralization processes that form reflectors.[26,27] Such reflectors are often characterized by layered structures, bound together by inter-molecular forces, including hydrogen bonds and aromatic stacking interactions. This anisotropic structure may result in crystal orientation dependent optical activity, a phenomenon known as birefringence. Non-layered optically active biogenic materials are also naturally available.[28,29] A notable example is riboflavin, whose crystals are found in the reflective tapetum lucidum layer in the eyes of cats and lemurs.[30,31]

The natural diversity of metal–organic crystals has inspired several studies, examining the optical properties of novel metal–organic and semi-organic systems. Zinc-based metal–organic crystals, for example, were found to display photoactuation behavior of jumping, rolling, and swelling upon UV irradiation.[32] Other studies have explored the non-linear optical properties of bioinspired phenylalanine- and cysteine-based metal–organic crystals,[33,34] and of metal–organic frameworks.[35,36]

In this context, Cu and Zn are ubiquitous in both biological and synthetic metal–organic systems. More specifically,

[a] *Shmunis School of Biomedicine and Cancer Research, George S. Wise Faculty of Life Sciences, Tel Aviv University, Tel Aviv 6997801, Israel*
[b] *Sagol School of Neuroscience, Tel Aviv University, Tel Aviv 6997801, Israel*
[c] *Department of Materials Science and Engineering, Iby and Aladar Fleischman Faculty of Engineering, Tel Aviv University, Tel Aviv 6997801, Israel. E-mail: ehudg@post.tau.ac.il*
[d] *Department of Molecular Chemistry and Materials Science, Weizmann Institute of Science, Rehovoth 7610001, Israel. E-mail: leeor.kronik@weizmann.ac.il*
[e] *Department of Physical Chemistry, School of Chemistry and The Sackler Centre for Computational Molecular and Materials Science, The Raymond and Beverly Sackler Faculty of Exact Sciences, Tel Aviv University, Tel Aviv 6997801, Israel. E-mail: odedhod@tauex.tau.ac.il*
[f] *Department of Mechanical and Industrial Engineering, University of Massachusetts, Amherst, Massachusetts 01003, USA*
[g] *Materials Science and Engineering Graduate Program, University of Massachusetts, Amherst, Massachusetts 01003, USA*

† Electronic supplementary information (ESI) available. See DOI: https://doi.org/10.1039/d4ma00999a

copper-metalloproteins play a crucial role in many biochemical reactions, *e.g.*, electron transfer in cellular respiration processes,[37] whereas zinc is known to structurally stabilize various metalloproteins and to participate in biochemical catalysis.[38] This makes them interesting candidates for investigation in bio-inspired systems. In this respect, the stable Cu^{2+} ion, with its $3d^9$ electronic configuration, has one unpaired electron that can form open-shell singlet or triplet spin configurations, depending on the surrounding chemical environment. Conversely, the stable Zn^{2+} ion has a $3d^{10}$ electronic configuration that can facilitate the formation of stable closed shell complexes. These properties can be harnessed to design bioinspired metal–organic crystals with enhanced electronic and optical properties.

The incorporation of copper and zinc ions within phenylalanine crystals transforms the native three-dimensional molecular framework into anisotropic layered structures (marked as Phe–Cu and Phe–Zn, respectively; see Table 1). Learning from the biological function of such layered molecular crystals, we postulate that they have the potential to exhibit reflective optical properties.[39,40] In contrast, replacing phenylalanine with cysteine, the cysteine–zinc (Cys–Zn) crystal forms a non-layered structure, like its native form.[41] This provides an opportunity to investigate the effect of metal ion incorporation on the structure of amino acid crystals, and its correlation with the resulting electronic, magnetic, and optical properties.

Inspired by these findings, in the present work we apply first-principles computational methods to study material properties of Phe–Cu/Zn and Cys–Cu/Zn crystals. In one experimentally accessible case, we also verify the computational predictions *via* refractive index measurements. We find that the incorporation of metal ions plays a significant role in crystal structure and morphology determination, which in turn affects the refractive properties of the studied crystals, with higher birefringence and anisotropy found for layered structures. Apart from this indirect effect, in some cases the metal ions are found to contribute directly to the dielectric response and therefore to the refractive index within a given crystal structure. These findings advance our understanding of structure–function relationships in bio-inspired metal–organic systems, aiming towards the rational design of optical materials with tunable properties for various applications in photonics.

2. Materials and methods

2.1. Crystal structures and morphological characterization

As input to first-principles calculations, we used known X-ray diffraction (XRD) crystal structures taken from the Cambridge Crystallographic Data Centre (CCDC). Extensive structural and morphological analyses can be found in the references appearing in Table 1, where XRD structure determination is available for all crystals considered and scanning electron microscopy and optical microscopy data are available for Phe–Cu and Phe–Zn.

Table 1 Crystal structures studied in this work

Crystal	CCDC number
L-Phenylalanine (Phe)[42,43]	1012982
L-Phenylalanine–Cu (Phe–Cu)[39]	1871975
L-Phenylalanine–Zn (Phe–Zn)[40]	1850564
L-Cysteine (Cys)[44]	1204446
L-Cysteine–Zn (Cys–Zn)[41]	708400

Metal-free structures were obtained by removing the metallic moieties from the optimized Phe–Cu and Cys–Zn crystal coordinates. In order to compare different metal types in the crystals and their effect on the refractive index, Cys–Cu was also examined by replacing the Zn with Cu in the crystal coordinates.

2.2. Density functional theory calculations

First-principles density functional theory (DFT) calculations were performed using the Vienna *ab initio* Simulation Package (VASP), version 6.2.1, which uses planewaves to address valence electrons and the projected augmented wave (PAW) method to address the ionic cores.[45–47] Geometry optimization of all crystal structures was carried out using the Perdew–Burke–Ernzerhof (PBE) generalized gradient exchange–correlation density functional approximation,[48] augmented by Tkatchenko–Scheffler van der Waals (TS-vdW) long-range dispersion interactions.[49] The Brillouin zones of all examined crystals were sampled using a Monkhorst–Pack[50] *k*-point grid of $5 \times 5 \times 5$, with a plane wave energy cutoff of 700 eV. Convergence tests against both parameters are presented in Fig. S1 and S2 of the ESI.† Forces were converged to 5×10^{-4} eV Å^{-1}.

For the metal-containing crystals, optimization was performed separately for each spin state (open-shell singlet or triplet for copper and closed- or open-shell singlet for zinc). Following optimization, the electronic structure was calculated using both PBE and the screened-exchange hybrid density functional of Heyd, Scuseria, and Ernzerhof (HSE06, henceforth referred to as HSE).[51,52] This approach was found to produce reliable results in molecular crystals, with respect to electronic structure and geometry optimization.[53] The refractive index (RI) was determined from the static ion-clamped dielectric matrix, calculated as a response to an external electric field of 0.001 eV Å^{-1}.[54]

2.3. Phenylalanine–copper crystals preparation and refractive index measurement

Phenylalanine–copper (Phe–Cu) crystals were grown according to the method described in ref. 39. Large crystals (0.5–1 mm in length) were chosen for performing the measurements.

The refractive index of the Phe–Cu crystal was measured by immersion oil and ellipsometry. Immersion oils of refractive indices ranging from 1.60 to 1.65 were cast onto Phe–Cu crystals deposited on a quartz surface. The samples were then imaged under optical microscopy and once the refractive index of the oil matched that of the crystal, the boundaries between them became indistinct and essentially invisible. For the ellipsometry measurements, single crystals of Phe–Cu were deposited on a silicon wafer (with a native oxide layer of $\sim$5 nm) and measured using a commercial imaging ellipsometer (Accurion EP4 equipped with a 10X objective) at 50 degrees. This allows for measurement of both in-plane and out-of-plane components of the refractive index. Rotating-compensator-based

analysis of the spectral dependence of the ellipsometric quantities Δ and Ψ was performed to yield the refractive indices.

3. Results and discussion

3.1. Geometry optimization

We first performed geometry optimization for the native amino-acid and metal–amino-acid crystal structures using DFT (see Section 2.2 above). The optimizations resulted in small changes in the lattice parameters, of the order of several percent at most, with respect to experimental coordinates obtained by X-ray crystallography (see Fig. 1a–d and Tables S1 and S2 in the ESI†). In addition, we performed optimizations of the above-mentioned artificial Cys–Cu structure and the metal-free structures constructed from the Phe–Cu and Cys–Zn coordinates (see Fig. 1e and f), in order to explore the structural and dielectric roles of the metal ions.

Both Phe–Cu and Phe–Zn adopt a layered structure, with the metallic ions "sandwiched" between the organic Phenyl backbone molecules, which are in turn stabilized by aromatic interactions and hydrogen bonds.[39,40] These "sandwich" layers then stack in the *c*-axis to form a macroscopic crystal. In contrast, Cys–Zn adopts a more isotropic three-dimensional crystal structure.[41]

3.2. Exploration of the relative energetic stability of different spin states

Aiming to identify the electronic ground state of each metal-containing crystal, we explored several low-spin states, including the closed shell, open-shell singlet, and triplet states, according to metal type. To that end, we performed separate geometry optimizations of each metal-containing crystal at the different spin states and compared their total energies – see Tables S3 and S4 in the ESI.† We focus on the results obtained from the HSE functional, which is known to provide an improved description of the electronic properties of metal-containing crystals, compared to the PBE functional.[55]

For the Phe–Cu crystal, the open-shell singlet state (with antiferromagnetic spin ordering between the metal centers) exhibits lower total energy than the triplet state (with ferromagnetic spin ordering) by ∼5 meV per unit cell, equivalent to a temperature of ∼50 K. This small energy difference implies weak magnetic coupling between the metal centers, with the open-shell singlet state (antiferromagnetic ordering) dominating the magnetic regime at temperatures lower than ∼50 K and the triplet state (ferromagnetic ordering) expected to play a role above that temperature, as discussed in ref. 39. In Phe–Zn systems, the closed shell structure displays a total energy lower by ∼0.52 eV per unit cell compared to the open-shell singlet structure, indicating a strong preference for the closed shell structure. This is to be expected, as the zinc ions in the crystal are in the +2 oxidation state and thus contain a full d-orbital shell, leading to a preference towards the closed shell spin configuration.

For the Cys–Cu crystal, the triplet spin state (with ferromagnetic spin ordering between the copper atoms) was found to be more stable than the open-shell singlet states (with antiferromagnetic spin ordering between the copper atoms) by ∼0.15 eV per unit cell, indicating that the triplet state is dominant.

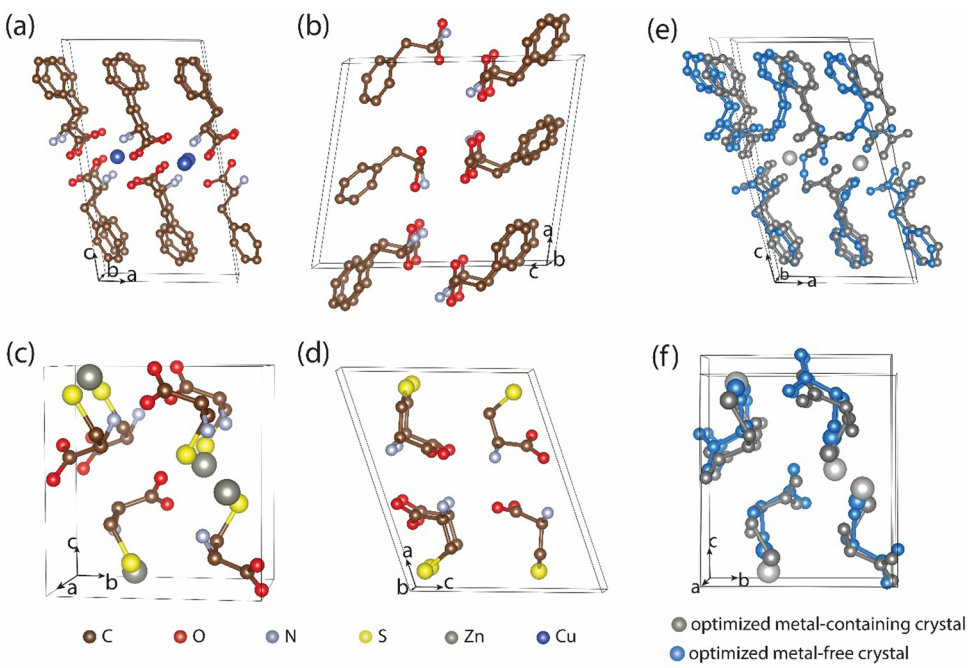

Fig. 1 Optimized structures of (a) Phe–Cu, (b) Phe in its native (monoclinic) structure, (c) Cys–Zn, (d) Cys in its native (monoclinic) structure. Hydrogen atoms are omitted for clarity. Atomic color coding appears near the bottom of panels (c) and (d). (e) and (f) A comparison between metal-containing Phe–Cu and Cys–Zn, and their metal-free analogues arising from the same parent structure (grey and blue, respectively).

For the Cys–Zn crystal, the initially open-shell singlet calculation converges to the closed shell result, indicating a much more stable closed shell structure, as expected for Zn^{2+} ions.

3.3. Exploration of the effect of metallic ions on the crystal structure

Next, we evaluate the effect of the metal ions on the crystal structure. As explained in Section 3.1, we removed the metal ions from the metal-containing structures and reoptimized the obtained metal-free structures. We emphasize that the latter are of different structure than that of the corresponding native crystal comprised of the same molecular building blocks. Metal ion removal from the crystal leads to significant lattice distortion (see Fig. 1e and f). Specifically, the *a*-axis length of the metal-free phenylalanine (''Phe metal-free'') crystal decreases by 1%, whereas the *b*- and *c*-axis lengths increase by 7% and 3%, respectively, resulting in a unit cell volume increase of 6%. For the metal-free cysteine (''Cys metal-free'') crystal, the *a*- and *b*-axis lattice parameters were found to decrease by 12% and 2%, respectively, whereas the *c*-axis length increased by 12%, resulting in a reduction of 3% in the overall unit cell volume.

To evaluate the role that metal ions play in determining structural stability, we calculate the Gibbs free energy of formation (ΔG),[56,57] while accounting for chemical composition. We use $\Delta G = E_{tot} - \chi_i\mu_i$, where E_{tot} is the total energy of a given structure, χ_i is the molar fraction of constituent atom i in this structure, and μ_i is its chemical potential, obtained for the bulk material at the same level of theory (see Table S5 in the ESI†). This approach considers the relative contribution of the constituent atoms to the total energy of the system and allows for a relatively straightforward qualitative comparison of systems containing different types of atoms. The results are summarized in Fig. 2. We find that for both Phe- and Cys-based systems, the metal-containing structures are considerably more stable than the non-metal-containing counterparts – in either the artificial metal-free structure or the naturally occurring monoclinic one.

Based on the above, we conclude that the metal ions play a critical role in stabilizing the non-native structure and, furthermore, significantly influence its detailed lattice parameters and atom arrangement.

3.4. Refractive index analysis – effects of crystal structure and metallic moieties

We now turn to examining the role that metal atoms play in the refractive properties of the crystals. Computed RI values for the three crystal axes (using HSE, with PBE values given in the ESI†), as well as their average, are given in Fig. 3 for the lowest-energy spin configuration of all materials under study. For the phenylalanine-based systems, the effect of the metallic atom appears to be minor. The average RI calculated for Phe–Cu and Phe–Zn is 1.63 and 1.65, respectively, and it remains 1.65 for the metal-free Phe-based crystal, in either the artificial or the native monoclinic structure. For the latter, this value is in good agreement with the experimental value of 1.68, measured in an aqueous solution.[58] For the Cys-based crystals, the picture is different. The average RI values of Cys–Cu and Cys–Zn are

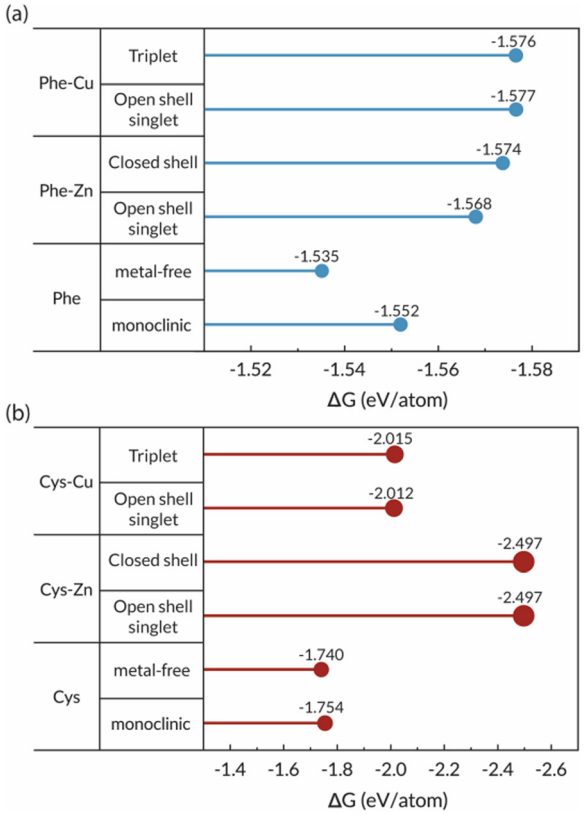

Fig. 2 Gibbs free energy of formation, ΔG, for the (a) Phe-based and (b) Cys-based crystals under study, calculated using the HSE functional.

found to be 1.73 and 1.72, respectively, compared to 1.65 for the artificial metal-free structure and 1.58 for the native monoclinic structure. In other words, about half of the increase due to the metal atom arises from the different crystal structure, whereas the other half is a direct result of the polarizability contribution of the metal atoms. We further note that RI values for other spin configurations of all materials are given in Table S6 of the ESI.† In general, the spin configuration has a minor effect on the RI, except in the case of Cys–Cu, where the open-shell singlet configuration is metallic and therefore its dielectric response is inherently different.

We also note that, as expected for molecular crystals exhibiting significant structural anisotropy,[9,11,16–18] birefringence was found in the Phe-based systems. For example, in the ''sandwich-like'' Phe–Cu crystal structure (Fig. 1), RI calculations yielded values of n_{fast} = 1.60 and n_{slow} = 1.70, *i.e.*, a birefringence value of Δn = 0.1, or approximately 6%, which is lower than that found in common biogenic or bio-inspired reflectors, such as guanine (Δn = 25%)[13] and theophylline (Δn = 15%).[22] For the native monoclinic Phe crystal with three structurally distinct axes (leading to a more anisotropic structure, compared to Phe–Cu), the calculated RI values are n_x = 1.65, n_y = 1.55, and n_z = 1.74.

3.5. Experimental measurement of the refractive index of the Phe–Cu crystal

In order to verify the RI computational results, Phe–Cu crystals were grown experimentally (unfortunately, Phe–Zn, Cys–Cu,

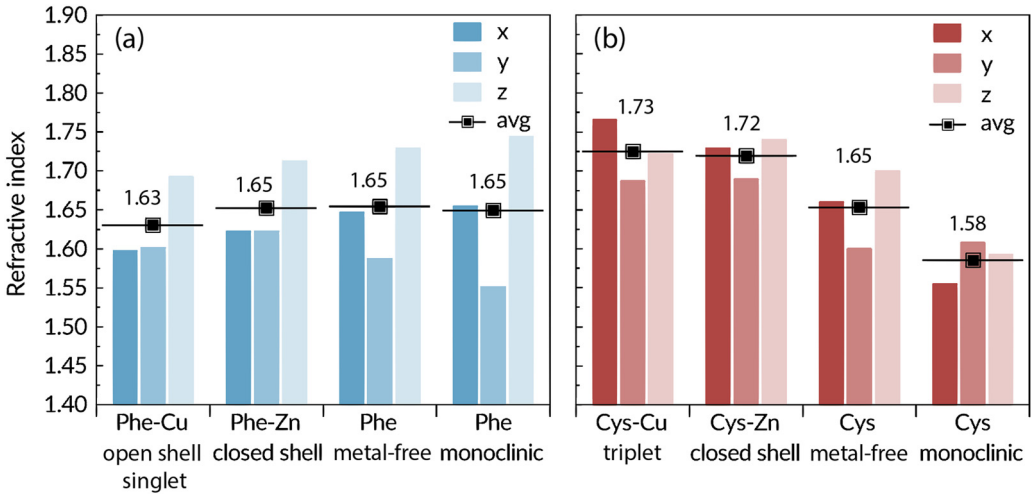

Fig. 3 RI of the (a) Phe-based and (b) Cys-based crystals under study (along the axes and average value), calculated using the HSE functional. For the metal–amino-acid crystals, the lowest energy spin states (open-shell singlet for Phe–Cu, triplet for Cys–Cu, closed shell for Phe–Zn and Cys–Zn) are presented.

and Cys–Zn crystals of a size large enough for reliable optical measurements were not obtained). Average RI values were then measured by immersion oil matching. Without immersion oil, the crystals are clearly observed, and the edges of the crystals are visible against the background (Fig. 4, left column). With immersion oil of RI 1.66 (Fig. 4, middle column), the crystals appear to be almost invisible, indicating that the RI of the oil is close to that of the crystals. With immersion oil of RI 1.64 (Fig. 4, right column), the crystals in the field of view seem invisible, indicating that the refractive index of the oil matches that of the crystals. This method is useful for characterizing the in-plane refractive index of the crystals. Ellipsometry measurements yielded n_{fast} = 1.63 ± 0.01 and n_{slow} = 1.71 ± 0.01 for the in-plane and out-of-plane refractive indices, respectively. These results closely agree with the above-stated calculated values of n_{fast} = 1.61 and n_{slow} = 1.71.

4. Conclusions

We have investigated the refractive properties of metal–amino acid crystals, focusing on factors influencing the RI, namely the crystal structure, inclusion of metal ions, and spin state. We found that the inclusion of metallic ions in the lattice has a

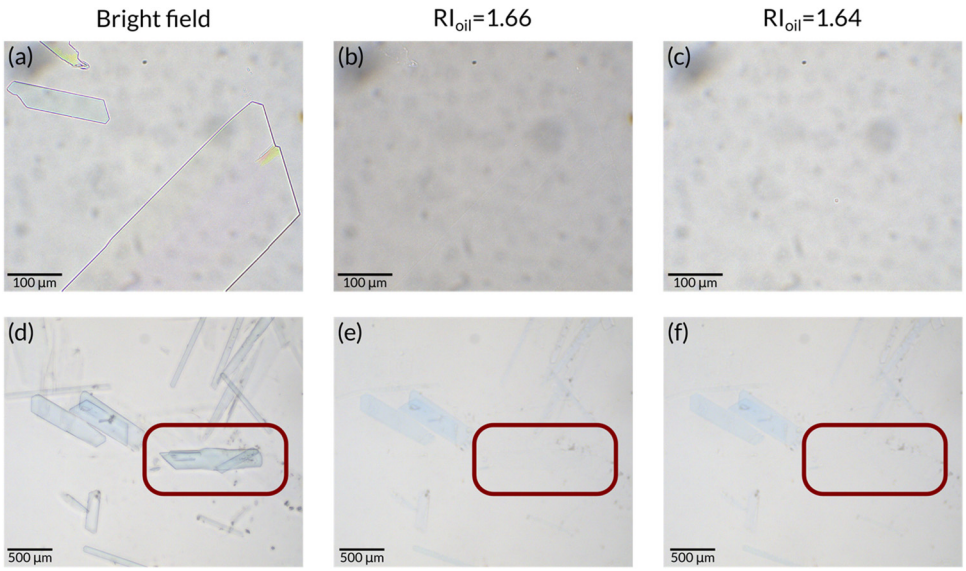

Fig. 4 Optical microscope images of Phe–Cu crystals under bright field illumination. Left column (a) and (d): no immersion oil. Middle column (b) and (e): immersion oil with an RI of 1.66. Right column (c) and (f): immersion oil with an RI of 1.64. Top (a)–(c) and bottom (d)–(f) rows present results for different crystals. The red rectangle represents an area of interest, containing a Phe–Cu crystal (d). The crystal becomes invisible once the refractive index of the immersion oil matches that of the crystal (f).

significant impact on the crystal structure and promotes its stability. We found that the metal ions have a small effect on the RI of phenylalanine-based crystals, but a significant effect on cysteine-based crystals. The latter effect arises both from structural changes induced by the metal ions and by their direct contribution to the dielectric response. These results demonstrate that inclusion of metal atoms in bio-inspired molecular crystals offers a flexible platform for the design of novel materials with desired optical features.

Data availability

Data supporting the findings presented in the article have been included as part of the main text and ESI.† Any additional data will be provided by the authors on reasonable request.

Conflicts of interest

There are no conflicts to declare.

Acknowledgements

M. C.-G. is grateful to the Azrieli Foundation for the award of an Azrieli International Postdoctoral Fellowship. E. G. acknowledges support of the ISF Israel-China program under grant no. 3246/23. L. K. acknowledges support by the Aryeh and Mintzi Katzman Professorial Chair and the Helen and Martin Kimmel Award for Innovative Investigation. O. H. is grateful to the Heinemann Chair in Physical Chemistry and acknowledges partial computational support from the Tel Aviv University Center for Nanoscience and Nanotechnology. Computational resources were provided by the Weizmann Institute of Science at Chemfarm. The authors would also like to thank Prof. Dan Oron of the Weizmann Institute of Science for his help with the experimental measurements.

References

1 S. Tadepalli, J. M. Slocik, M. K. Gupta, R. R. Naik and S. Singamaneni, Bio-Optics and Bio-Inspired Optical Materials, *Chem. Rev.*, 2017, **117**, 12705–12763.
2 Z. W. Han, Z. Wang, X. M. Feng, B. Li, Z. Z. Mu, J. Q. Zhang, S. C. Niu and L. Q. Ren, Antireflective Surface Inspired from Biology: A Review, *Biosurf. Biotribol.*, 2016, **2**, 137–150.
3 K. Tao, P. Makam, R. Aizen and E. Gazit, Self-Assembling Peptide Semiconductors, *Science*, 2017, **358**, eaam9756.
4 M. Amit, S. Yuran, E. Gazit, M. Reches and N. Ashkenasy, Tailor-Made Functional Peptide Self-Assembling Nanostructures, *Adv. Mater.*, 2018, **30**, 1707083.
5 U. G. K. Wegst, H. Bai, E. Saiz, A. P. Tomsia and R. O. Ritchie, Bioinspired Structural Materials, *Nat. Mater.*, 2014, **14**, 23–36.
6 Y. Fu, C. A. Tippets, E. U. Donev and R. Lopez, Structural Colors: From Natural to Artificial Systems, *WIREs Nanomed. Nanobiotechnol.*, 2016, **8**, 758–775.
7 E. Dujardin and S. Mann, Bio-Inspired Materials Chemistry, *Adv. Mater.*, 2002, **14**, 775.
8 B. A. Palmer, D. Gur, S. Weiner, L. Addadi and D. Oron, The Organic Crystalline Materials of Vision: Structure–Function Considerations from the Nanometer to the Millimeter Scale, *Adv. Mater.*, 2018, **30**, 1–10.
9 A. Wagner, Q. Wen, N. Pinsk and B. A. Palmer, Functional Molecular Crystals in Biology, *Isr. J. Chem.*, 2021, **61**, 668–678.
10 L. Addadi, L. Kronik, L. Leiserowitz, D. Oron and S. Weiner, Organic Crystals and Optical Functions in Biology: Knowns and Unknowns, *Adv. Mater.*, 2024, 2408060.
11 M. F. Land, The Physics and Biology of Animal Reflectors, *Prog. Biophys. Mol. Biol.*, 1972, **24**, 75–106.
12 A. Hirsch, D. Gur, I. Polishchuk, D. Levy, B. Pokroy, A. J. Cruz-Cabeza, L. Addadi, L. Kronik and L. Leiserowitz, ''Guanigma'': The Revised Structure of Biogenic Anhydrous Guanine, *Chem. Mater.*, 2015, **27**, 8289–8297.
13 A. Levy-Lior, E. Shimoni, O. Schwartz, E. Gavish-Regev, D. Oron, G. Oxford, S. Weiner and L. Addadi, Guanine-Based Biogenic Photonic-Crystal Arrays in Fish and Spiders, *Adv. Funct. Mater.*, 2010, **20**, 320–329.
14 D. Gur, B. A. Palmer, S. Weiner and L. Addadi, Light Manipulation by Guanine Crystals in Organisms: Biogenic Scatterers, Mirrors, Multilayer Reflectors and Photonic Crystals, *Adv. Funct. Mater.*, 2017, **27**, 1603514.
15 J. Teyssier, S. V. Saenko, D. van der Marel and M. C. Milinkovitch, Photonic Crystals Cause Active Colour Change in Chameleons, *Nat. Commun.*, 2015, **6**, 6368.
16 G. Zhang, A. Hirsch, G. Shmul, L. Avram, N. Elad, V. Brumfeld, I. Pinkas, Y. Feldman, R. Ben Asher, B. A. Palmer, L. Kronik, L. Leiserowitz, S. Weiner and L. Addadi, Guanine and 7,8-Dihydroxanthopterin Reflecting Crystals in the Zander Fish Eye: Crystal Locations, Compositions, and Structures, *J. Am. Chem. Soc.*, 2019, **141**, 19736–19745.
17 A. Böhm and G. Pass, The Ocelli of Archaeognatha (Hexapoda): Functional Morphology, Pigment Migration and Chemical Nature of the Reflective Tapetum, *J. Exp. Biol.*, 2016, **219**, 3039–3048.
18 B. A. Palmer, A. Hirsch, V. Brumfeld, E. D. Aflalo, I. Pinkas, A. Sagi, S. Rosenne, D. Oron, L. Leiserowitz, L. Kronik, S. Weiner and L. Addadi, Optically Functional Isoxanthopterin Crystals in the Mirrored Eyes of Decapod Crustaceans, *PNAS*, 2018, **115**, 2299–2304.
19 A. Pirie, Crystals of Riboflavin Making up the Tapetum Lucidum in the Eye of a Lemur, *Nature*, 1959, **183**, 985–986.
20 R. Vaz, M. F. Frasco and M. G. F. Sales, Photonics in Nature and Bioinspired Designs: Sustainable Approaches for a Colourful World, *Nanoscale Adv.*, 2020, **2**, 5106–5129.
21 F. Chen, Y. Huang, R. Li, S. Zhang, B. Wang, W. Zhang, X. Wu, Q. Jiang, F. Wang and R. Zhang, Bio-Inspired Structural Colors and Their Applications, *Chem. Commun.*, 2021, **57**, 13448.
22 A. Niazov-Elkan, M. Shepelenko, L. Alus, M. Kazes, L. Houben, K. Rechav, G. Leitus, A. Kossoy, Y. Feldman, L. Kronik, P. G. Vekilov and D. Oron, Surface-Guided Crystallization of Xanthine Derivatives for Optical Metamaterial Applications, *Adv. Mater.*, 2024, **36**, 2306996.

23 A. Hirsch, B. A. Palmer, A. Ramasubramaniam, P. A. Williams, K. D. M. Harris, B. Pokroy, S. Weiner, L. Addadi, L. Leiserowitz and L. Kronik, Structure and Morphology of Light-Reflecting Synthetic and Biogenic Polymorphs of Isoxanthopterin: A Comparison, *Chem. Mater.*, 2019, **31**, 4479–4489.
24 T. Gorniak, T. Haraszti, H. Suhonen, Y. Yang, A. Hedberg-Buenz, D. Koehn, R. Heine, M. Grunze, A. Rosenhahn and M. G. Anderson, Support and Challenges to the Melanosomal Casing Model Based on Nanoscale Distribution of Metals within Iris Melanosomes Detected by X-Ray Fluorescence Analysis, *Pigm. Cell Melanoma Res.*, 2014, **27**, 831–834.
25 Y. Liu and J. D. Simon, Metal–Ion Interactions and the Structural Organization of Sepia Eumelanin, *Pigm. Cell Res.*, 2005, **18**, 42–48.
26 A. Palumbo, M. d'Ischia, G. Misuraca and G. Prota, Effect of Metal Ions on the Rearrangement of Dopachrome, *Biochim. Biophys. Acta, Gen. Subj.*, 1987, **925**, 203–209.
27 J. M. Bowness, R. A. Morton, M. H. Shakir and A. L. Stubbs, Distribution of Copper and Zinc in Mammalian Eyes. Occurrence of Metals in Melanin Fractions from Eye Tissues, *Biochem. J.*, 1952, **51**, 521–530.
28 M. Guerain, F. Affouard, C. Henaff, C. Dejoie, F. Danède, J. Siepmann, F. Siepmann and J.-F. Willart, Structure Determination of Riboflavin by Synchrotron High-Resolution Powder X-Ray Diffraction, *Acta Crystallogr., Sect. C: Struct. Chem.*, 2021, **77**, 800–806.
29 C. J. H. Smalley, C. E. Hughes, M. Hildebrand, R. Aizen, M. Bauer, A. Yamano, D. Levy, S. K. Mirsky, N. T. Shaked, M. T. Young, U. Kolb, E. Gazit, L. Kronik and K. D. M. Harris, Understanding the Solid-State Structure of Riboflavin through a Multitechnique Approach, *Cryst. Growth Des.*, 2024, **24**, 6256–6266.
30 A. Pirie, Crystals of Riboflavin Making up the Tapetum Lucidum in the Eye of a Lemur, *Nature*, 1959, **183**, 985–986.
31 J. H. Elliot and S. Futterman, Fluorescence in the Tapetum of the Cat's Eye, *Arch. Ophthalmol.*, 1963, **70**, 531.
32 S. Khan, B. Dutta, S. Naaz, A. Choudhury, P.-A. Cazade, E. Kiely, S. Guerin, R. Medishetty and M. H. Mir, Regulating Photosalient Behavior in Dynamic Metal-Organic Crystals, *Commun. Chem.*, 2023, **6**, 150.
33 M. Shalini, M. Meena, R. S. Sundararajan, B. S. Ebinezer and T. C. Sabari Girisun, Spectral, Structural, Mechanical, Linear, and Nonlinear Optical Properties of L-Cysteine Hydrochloride Monohydrate Magnesium Sulphate (LCHMS) Single Crystals Synthesized by Slow Evaporation Method, *J. Mater. Sci.: Mater. Electron.*, 2023, **34**, 2058.
34 M. Meena, B. Samuel Ebinezer, R. S. Sundararajan, E. Manikandan, T. C. Sabari Girisun, M. Shalini and R. Natarajan, A Study on Novel Semi-Organic Material L-Phenylalanine Mixed with Cadmium Nitrate Single Crystals, *J. Mol. Liq.*, 2023, **390**, 123123.
35 C. Li, G. Qian and Y. Cui, Metal–Organic Frameworks for Nonlinear Optics and Lasing, *Inform. Funct. Mater.*, 2024, **1**, 125–159.
36 H. Yuan, X. Xu, Z. Qiao, D. Kottilil, D. Shi, W. Fan, Y. D. Yuan, X. Yu, A. Babusenan, M. Zhang and W. Ji, Tunable Nonlinear Optical Properties Based on Metal–Organic Framework Single Crystals, *Adv Opt. Mater.*, 2024, **12**, 2302405.
37 T. Tsang, C. I. Davis and D. C. Brady, Copper Biology, *Curr. Biol.*, 2021, **31**, R421–R427.
38 S. Clemens, The Cell Biology of Zinc, *J. Exp. Bot.*, 2022, **73**, 1688–1698.
39 A. K. Mondal, N. Brown, S. Mishra, P. Makam, D. Wing, S. Gilead, Y. Wiesenfeld, G. Leitus, L. J. W. Shimon, R. Carmieli, D. Ehre, G. Kamieniarz, J. Fransson, O. Hod, L. Kronik, E. Gazit and R. Naaman, Long-Range Spin-Selective Transport in Chiral Metal-Organic Crystals with Temperature-Activated Magnetization, *ACS Nano*, 2020, **14**, 16624–16633.
40 P. Makam, S. S. R. K. C. Yamijala, K. Tao, L. J. W. Shimon, D. S. Eisenberg, M. R. Sawaya, B. M. Wong and E. Gazit, Non-Proteinaceous Hydrolase Comprised of a Phenylalanine Metallo-Supramolecular Amyloid-like Structure, *Nat. Catal.*, 2019, **2**, 977–985.
41 J. N. Rebilly, P. W. Gardner, G. R. Darling, J. Bacsa and M. J. Rosseinsky, Chiral II–VI Semiconductor Nanostructure Superlattices Based on an Amino Acid Ligand, *Inorg. Chem.*, 2008, **47**, 9390–9399.
42 P. A. Williams, C. E. Hughes, A. B. M. Buanz, S. Gaisford and K. D. M. Harris, Expanding the Solid-State Landscape of L-Phenylalanine: Discovery of Polymorphism and New Hydrate Phases, with Rationalization of Hydration/Dehydration Processes, *J. Phys. Chem. C*, 2013, **117**, 12136–12145.
43 H. M. Cuppen, M. M. H. Smets, A. M. Krieger, J. A. van den Ende, H. Meekes, E. R. H. van Eck and C. H. Görbitz, The Rich Solid-State Phase Behavior of l-Phenylalanine: Disappearing Polymorphs and High Temperature Forms, *Cryst. Growth Des.*, 2019, **19**, 1709–1719.
44 M. M. Harding and H. A. Long, The Crystal and Molecular Structure of L-Cysteine, *Acta Crystallogr.*, 1968, **24**, 1096–1102.
45 G. Kresse and J. Furthmüller, Efficient Iterative Schemes for Ab Initio Total-Energy Calculations Using a Plane-Wave Basis Set, *Phys. Rev. B: Condens. Matter Mater. Phys.*, 1996, **54**, 11169–11186.
46 G. Kresse and J. Furthmüller, Efficiency of Ab-Initio Total Energy Calculations for Metals and Semiconductors Using a Plane-Wave Basis Set, *Comput. Mater. Sci.*, 1996, **6**, 15–50.
47 G. Kresse and D. Joubert, From Ultrasoft Pseudopotentials to the Projector Augmented-Wave Method, *Phys. Rev. B: Condens. Matter Mater. Phys.*, 1999, **59**, 1758.
48 J. P. Perdew, K. Burke and M. Ernzerhof, Generalized Gradient Approximation Made Simple, *Phys. Rev. Lett.*, 1996, **77**, 3865–3868.
49 A. Tkatchenko and M. Scheffler, Accurate Molecular van der Waals Interactions from Ground-State Electron Density and Free-Atom Reference Data, *Phys. Rev. Lett.*, 2009, **102**, 073005.
50 H. J. Monkhorst and J. D. Pack, Special Points for Brillouin-Zone Integrations, *Phys Rev B: Solid State*, 1976, **13**, 5188–5192.

51 J. Heyd, G. E. Scuseria and M. Ernzerhof, Hybrid Functionals Based on a Screened Coulomb Potential, *J. Chem. Phys.*, 2003, **118**, 8207.
52 J. Heyd; G. E. Scuseria and M. Ernzerhof Erratum: "Hybrid Functionals Based on a Screened Coulomb Potential" [J. Chem. Phys. 118, 8207 (2003)]. *J. Chem. Phys.* 2006, 124, 219906.
53 L. Kronik and A. Tkatchenko, Understanding Molecular Crystals with Dispersion-Inclusive Density Functional Theory: Pairwise Corrections and Beyond, *Acc. Chem. Res.*, 2014, **47**, 3208–3216.
54 I. Souza, J. Íñiguez and D. Vanderbilt, First-Principles Approach to Insulators in Finite Electric Fields, *Phys. Rev. Lett.*, 2002, **89**, 117602.
55 S. Kümmel and L. Kronik, Orbital-Dependent Density Functionals: Theory and Applications, *Rev. Mod. Phys.*, 2008, **80**, 3–60.
56 T. Dumitrică, M. Hua and B. I. Yakobson, Endohedral Silicon Nanotubes as Thinnest Silicide Wires, *Phys. Rev. B: Condens. Matter Mater. Phys.*, 2004, **70**, 241303.
57 V. Barone, O. Hod and G. E. Scuseria, Electronic Structure and Stability of Semiconducting Graphene Nanoribbons, *Nano Lett.*, 2006, **6**, 2748–2754.
58 T. L. McMeekin, M. L. Groves and N. J. Hipp, Refractive Indices of Amino Acids, Proteins, and Related Substances, *Adv. Chem.*, 1964, **44**, 54–66.